[16] P. Tracqui, G. C. Cruywagen, D. E. Woodward, G. T. Bartoo, J. D. Murray and E. C. Alvord Jr, *A mathematical model of glioma growth: the effect of chemotherapy on spatio-temporal growth,* Cell Proliferat. **28** (1995) 17–31.
[17] J. P. Ward and J. R. King, *Mathematical modelling of drug transport in tumour multicell spheroids and monolayer cultures,* Mathematical Biosciences **181** (2003) 177–207.
[18] C. Walker and G. Webb, *Global existence of classical solutions for a haptotaxis model,* SIAM Journal on Mathematical Analysis **38** (2007) 1694–1713.

J. R. Branco
CMUC & Polytechnic Institute of Coimbra, ISEC, DFM, Coimbra, Portuga
E-mail address: jrbranco@isec.pt

J. A. Ferreira
CMUC, Department of Mathematics, University of Coimbra
E-mail address: ferreira@mat.uc.pt

P. de Oliveira
CMUC, Department of Mathematics, University of Coimbra
E-mail address: poliveir@mat.uc.pt

G. Pena
CMUC, Department of Mathematics, University of Coimbra
E-mail address: gpena@mat.uc.pt

Pré-Publicações do Departamento de Matemática
Universidade de Coimbra
Preprint Number 16–48

GLIOMA GROWTH: A MATHEMATICAL APPROACH FOR CHEMOTHERAPY PROTOCOLS

J. R. BRANCO, J. A. FERREIRA, P. DE OLIVEIRA AND G. PENA

Abstract: In this paper we analyse properties of a nonlinear mathematical model that describes the evolution of brain tumour cells under the effect of a chemotherapy drug, considering the viscoelastic behaviour of the brain. Under suitable regularity conditions we establish upper bounds for an energy functional of the system, with respect to the L^2 norm, leading to the stability of the model. Chemotherapy treatment protocols based on stronger assumptions on the drug and cell kinetics are also proposed with the purpose of controlling tumour growth. These protocols are based on suitable estimates for the mass of tumour cells in the system after chemotherapy sessions. A numerical method based on finite differences and finite elements is introduced and its stability properties are analysed. The qualitative behaviour of the solutions of the system is explored and discussed.

Keywords: Glioma, chemotherapy, numerical simulation, treatment protocols.

1. Introduction

Tumours are the uncontrolled growth of abnormal cells. Gliomas, which are a special case of brain tumours, present a high mortality rate, giving six months to one year of life expectancy once diagnosed (even undergoing treatment). Medical doctors believe that a reason for the inefficiency of such treatments lies in the high motility of the tumour cells.

The modelling of migration and proliferation of tumour cells has received attention in the scientific community during the last decades. The simplest approach is to model the motion of tumour cells by passive diffusion. This was first proposed in [9], who introduced a partial differential equation built upon a mass conservation law. Later work [3, 4], based on the principles followed in [9], modelled tumour cells as having two possible phenotypes (or states), proliferative and migratory, allowing cells to switch between both phenotypes. However, such models do not take into account the effect of the extracellular matrix or of any chemical agent in the surroundings of the

Received December 5th, 2016.
This work was partially supported by the Centre for Mathematics of the University of Coimbra – UID/MAT/00324/2013, funded by the Portuguese Government through FCT/MEC and co-funded by the European Regional Development Fund through the Partnership Agreement PT2020.

brain/tumour cells for their motion. Scientific evidence has shown that three major phenomena come into play in this context, besides passive diffusion of cells: chemotaxis, haptotaxis and durotaxis. The chemotactic effect models motion driven by a concentration gradient of a chemical produced by tumour cells' matrix degrading enzymes (MDE), haptotaxis accounts for motion directed in response to the degradation of the extracellular matrix (ECM) by MDE and durotaxis represents cells' motion driven by gradients in ECM stiffness. In the literature, models considering some of these effects can be found in [8, 15, 18].

The influence of stiffness in the diffusion of molecules in polymeric matrices was addressed in [5, 6]. Recent accumulated evidence of molecular biologists and experimentalists (see, for example, [13]) suggests that the mechanical properties of the ECM, stiffness and microstructure, have a crucial influence on cell motility and proliferation. In [1] a coupled system of ODE-PDE and an integro-differential equation, was used to represent invasion (by passive diffusion), proliferation and treatment of glioma cells, considering the different rigidity of gray and white matter. The authors obtained qualitative results in agreement with the medical literature. The influence of the stiffness and confinement of a 3D culture matrix was also studied in [11] and numerical simulations were compared with in vitro results. The inclusion of the stiffness effect properties brings another layer of complexity to these models: the geometry of the white and gray matter should be taken into account, see [14].

Once a brain tumour is diagnosed, several therapeutic approaches are usually followed, depending on the characteristics of the tumour. The most common treatments involve chemotherapy, radiotherapy or even resection. Chemotherapy (or radiotherapy) has also been incorporated in existing models for tumour growth. This has been accomplished by introducing an additional term in the partial differential system that removes cells at a rate depending on the concentration of a certain drug (or an amount of radiation, in the case of radiotherapy), [2, 10, 16].

The study of treatment protocols, based upon the partial differential systems that model chemotherapy effects in tumour growth, has also received some attention recently. In [1], the authors deduced, for a linear problem, bounds for different energies of the system. This allowed to create treatment protocols, based on suitable sufficient conditions, aiming to control the tumour growth. A more complex model was proposed in [2], introducing nonlinear terms for the coupling between drug concentration and tumour cells' removal.

so in (45) we obtain

$$B_1 \left\|u^{n+1}\right\|^2 + \Delta t\, C \left\|\nabla u^{n+1}\right\|^2 + B_2 \left\|v^{n+1}\right\|^2 + B_3 \left\|c^{n+1}\right\|^2 + 2\Delta t\, \delta \left\|\nabla c^{n+1}\right\|^2$$
$$\leq \|u^n\|^2 + \|v^n\|^2 + \|c^n\|^2 + \lambda \Delta t \left(\Delta t + \|\ker\|^2_{L^2(\mathbb{R}^+)}\right) \sum_{i=1}^{n} \left\|\nabla u^i\right\|^2$$
$$+ \Delta t (\mathrm{meas}(\Omega) g(t_{n+1}))^2. \quad (46)$$

It follows that

$$(1 + \Delta t C_1)\, \mathbb{E}_{n+1} \leq (1 + C_2)\, \mathbb{E}_n + \Delta t \big(\mathrm{meas}(\Omega) g(t_{n+1})\big)^2$$

and using a standard argument we obtain (23).

■

References

[1] J. R. Branco, J. A. Ferreira and P. de Oliveira, *Mathematical modelling of efficient protocols to control glioma growth,* Math Biosci. **255** (2014) 83–90.

[2] J. R. Branco, J. A. Ferreira, P. de Oliveira and G. Pena, *Chemotherapy for brain tumour: balance between frequency and intensity,* in Proceedings of the 2015 International Conference on Computational and mathematical Methods in Science and Engineering, Cadiz, Spain, July 6-10, 2015, Editor: J. Vigo Aguiar, (2015) 244–253.

[3] S. Fedotov and A. Iomin, *Migration and proliferation dichotomy in tumour-cell invasion,* Phys. Rev. Lett. **98**(118110) (2007) 1–4.

[4] S. Fedotov and A. Iomin, *Probabilistic approach to a proliferation and migration dichotomy in tumour cell invasion,* Phys. Rev. E **77**(1031911) (2008) 1–10.

[5] J. Ferreira, P. Oliveira, P. Silva and L. Simon, *Molecular transport in viscoelastic materials: mechanistic properties and chemical affinities,* SIAM Journal on Applied Mathematics **74** (2014) 1598–1614.

[6] J. Ferreira, M. Grassi, E. Gudiño and P. Oliveira, *A 3D model for mechanistic control drug release,* SIAM Journal on Applied Mathematics **74** (2014) 620–633.

[7] G. Franceschini, *The mechanics of human brain tissue,* PhD thesis, University of Trento, 2006.

[8] E. Keller and L. Segel, *Initiation of slime mold aggregation viewed as an instability,* Journal of Theoretical Biology, **26** (1970) 399–415.

[9] J. D. Murray, *Mathematical Biology,* Springer, 2002.

[10] E. S. Norris, J. R. King and H. M. Byrne, *Modelling the response of spatially structured tumours to chemotherapy: Drug kinetics,* Mathematical and Computer Modelling **43** (2006) 820–837.

[11] A. Pathak and S. Kumar, *Independent regulation of tumour cell migration by matrix stiffness and confinement,* Proceedings of the National Academy of Sciences **109** (2012) 10334–10339.

[12] A. Roniotis, K. Marias, V. Sakkalis and M. Zervakis, *Diffusive modelling of glioma evolution: a review,* J. Biomed. Eng. **3** (2010) 501–508.

[13] V. Seewaldt, *ECM stiffness paves the way for tumour cells,* Nature Medicine **20** (2014) 332–333.

[14] K. R. Swanson, E. C. Alvord Jr and J. D. Murray, *A quantitative model for differential motility of gliomas in grey and white matter,* Cell Proliferat. **33** (2000) 317–329.

[15] Y. Tao and M. Winkler, *Dominance of chemotaxis in a chemotaxis-haptotaxis model,* Nonlinearity **27** (2014) 1225–1239.

for $q \in V_h$ and $i \in \{n, n+1\}$. Therefore, system (43) is rewritten as

$$\begin{aligned}
A_1 \left\|u^{n+1}\right\|^2 &\leq \|u^n\|^2 - 2\Delta t\,\delta \left\|\nabla u^{n+1}\right\|^2 + \Delta t\beta_2 \left\|v^{n+1}\right\|^2 \\
&\quad + 2\Delta t^2 \sum_{i=1}^{n+1} \ker(t_{n+1} - t_i)(D_v \nabla u^i, \nabla u^{n+1}), \\
A_2 \left\|v^{n+1}\right\|^2 &\leq \|v^n\|^2 + \Delta t\beta_1 \left\|u^{n+1}\right\|^2, \\
A_3 \left\|c^{n+1}\right\|^2 &\leq \|c^n\|^2 - 2\Delta t\,\delta \left\|\nabla c^{n+1}\right\|^2 \\
&\quad - 2\Delta t \left(\frac{k(c^{n+1})(u^{n+1} + v^{n+1})}{\alpha} - g(t_{n+1}), c^{n+1}\right)
\end{aligned} \tag{44}$$

where $A_1 = 1 + \Delta t(2\beta_1 - \beta_2)$, $A_2 = 1 + \Delta t(2(\beta_2 - \rho) - \beta_1)$ and $A_3 = 1 + 2\Delta t M$.

From Young's inequality, one can show that

$$-2(k(c^{n+1})q, c^{n+1}) \leq \|k\|_\infty \left(\|q\|^2 + \left\|c^{n+1}\right\|^2\right)$$

for $q = u^{n+1}$ or $q = v^{n+1}$ and

$$2(g(t_{n+1}), c^{n+1}) \leq (\mathrm{meas}(\Omega) g(t_{n+1}))^2 + \left\|c^{n+1}\right\|^2.$$

Combining these last inequalities with (44) and summing all inequalities term by term, we obtain

$$\begin{aligned}
B_1 \left\|u^{n+1}\right\|^2 + B_2 \left\|v^{n+1}\right\|^2 + B_3 \left\|c^{n+1}\right\|^2 &\leq \|u^n\|^2 + \|v^n\|^2 + \|c^n\|^2 \\
- 2\Delta t\,\delta \left\|\nabla u^{n+1}\right\|^2 + 2\Delta t^2 \sum_{i=1}^{n+1} \ker(t_{n+1} - t_i)(D_v \nabla u^i, \nabla u^{n+1}) \\
- 2\Delta t\,\delta \left\|\nabla c^{n+1}\right\|^2 + \Delta t(\mathrm{meas}(\Omega) g(t_{n+1}))^2
\end{aligned} \tag{45}$$

where $B_1 = 1 + \Delta t(\beta_1 - \beta_2 - \frac{\|k\|_\infty}{\alpha})$, $B_2 = 1 + \Delta t(\beta_2 - 2\rho - \beta_1 - \frac{\|k\|_\infty}{\alpha})$ and $B_3 = 1 + 2\Delta t(M - \frac{\|k\|_\infty}{\alpha} - \frac{1}{2})$.

From Cauchy-Schwarz, Young and Hölder inequalities we get

$$\begin{aligned}
\Delta t \sum_{i=1}^{n+1} \ker(t_{n+1} - t_i)(D_v \nabla u^i, \nabla u^{n+1}) &\leq \lambda \left(\Delta t + \frac{\|\ker\|^2_{L^2(\mathbb{R}^+)}}{2}\right) \left\|\nabla u^{n+1}\right\|^2 \\
&\quad + \frac{\lambda}{2} \left(\Delta t + \|\ker\|^2_{L^2(\mathbb{R}^+)}\right) \sum_{i=1}^{n} \left\|\nabla u^i\right\|^2
\end{aligned}$$

In this paper we introduce the following model for the evolution of tumour cells and concentration of chemotherapy drug,

$$\begin{cases}
\dfrac{\partial u}{\partial t} + \nabla \cdot J_u = -\beta_1 u + \beta_2 v - k(c)u, & \text{in } \Omega \times (0, T], \\
\dfrac{\partial v}{\partial t} = \rho v + \beta_1 u - \beta_2 v - k(c)v, & \text{in } \Omega \times (0, T], \\
\dfrac{\partial c}{\partial t} + \nabla \cdot J_c = -\dfrac{k(c)}{\alpha}(u + v) + g(t) - Mc, & \text{in } \Omega \times (0, T],
\end{cases} \tag{1}$$

where $\Omega \subset \mathbb{R}^d$ $(d = 2, 3)$, u and v are the densities of migratory and proliferative cells, ρ is the proliferation rate, β_1 and β_2 are the phenotype switching rate parameters, J_u is the mass flux associated with cells' migration, c is the drug concentration, k is a nonnegative function of the concentration that represents the rate at which cells die due to the drug's effect, J_c is the mass flux for the drug, coefficient α is the measure of the rate of cell kill relative to the rate of drug degradation, g is a source term for the concentration and M is the washout effect for the drug. This model is an extension of the model proposed in [2] by adding integral terms to account for the rigidity of the brain tissue. The definitions and units of the model parameters are presented in Appendix A.

To study system (1) we start by establishing convenient energy estimates, see Section 2, as well as upper bounds for the total mass of cells in the system, see Section 3. While the first results are interesting from a mathematical point of view, they do not lead to treatment protocols. However, such protocols can be obtained with the latter upper bounds and some examples are presented in Section 3. Finally, in Section 4, we propose a numerical method to approximate the solution of the nonlinear system of equations. A stability analysis of the numerical method is also performed. Some numerical results showing the efficiency of the treatment protocols are presented in Section 5 followed by a brief discussion.

2. Model analysis

We assume that the drug diffuses according to Fick's law, that is, we define its flux as

$$J_c(t) = -D_c \nabla c(t), \tag{2}$$

where D_c represents the diffusion tensor of the drug. Regarding glioma cells, the fickian flux $J_F(t)$ is modified by adding a term $J_{NF}(t)$ that will take into

account that glioma cells spread more in a stiffer environment, see [11]. We define the total flux $J_u(t)$ by

$$J_u(t) = J_F(t) + J_{NF}(t). \tag{3}$$

The fickian flux of glioma cells, $J_F(t)$, is represented by

$$J_F(t) = -\tilde{D}\nabla u(t), \tag{4}$$

where $\tilde{D}$ stands for the diffusion tensor of glioma cells and the nonfickian flux $J_{NF}(t)$ is defined by

$$J_{NF}(t) = -\tilde{D}_v\nabla\sigma(t), \tag{5}$$

where σ represents the stress (the force per unit area) exerted by the extracellular matrix and $\tilde{D}_v$ represents the stress driven diffusion tensor, a diagonal tensor with negative entries.

To complete the definition of J_{NF}, a relation between the stress σ and the strain ε is adopted. Several viscoelastic models have been used in the literature to simulate the mechanical behaviour of the brain. In this work, we adopt a linear Kelvin-Voigt model consisting of a Hookean spring in series with a Kelvin body, as depicted in Figure 1, which shows an almost perfect

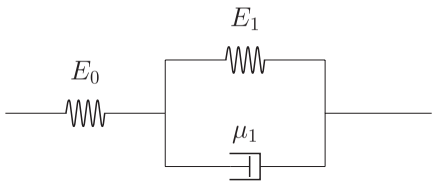

FIGURE 1. Kelvin-Voigt model: a Hookean spring in series with a Kelvin body.

agreement with experimental data [7]. We note that in case of strongly localised displacements of the brain tissue, that may occur in later stages of tumour development, nonlinear models can provide more realistic simulations.

The differential equation associated with the Kelvin-Voigt model is

$$\frac{\partial\sigma}{\partial t} + \beta\sigma = \alpha_1\varepsilon + \alpha_2\frac{\partial\varepsilon}{\partial t} \tag{6}$$

with

$$\beta = \frac{E_0 + E_1}{\mu_1}, \quad \alpha_1 = \frac{E_0E_1}{\mu_1}, \quad \alpha_2 = E_0,$$

Proof of Theorem 5: Let $w = u^{n+1}$, $z = v^{n+1}$ and $q = c^{n+1}$. From system (22) it follows

$$\begin{aligned}
\left\|u^{n+1}\right\|^2 &= (u^n, u^{n+1}) - \Delta t\left\|\sqrt{D}\nabla u^{n+1}\right\|^2 - \Delta t\beta_1\left\|u^{n+1}\right\|^2 + \Delta t\beta_2(v^{n+1}, u^{n+1}) \\
&\quad - \Delta t(k(c^n)u^{n+1}, u^{n+1}) + \Delta t^2\sum_{i=1}^{n+1}\ker(t_{n+1} - t_i)(D_v\nabla u^i, \nabla u^{n+1}), \\
\left\|v^{n+1}\right\|^2 &= (v^n, v^{n+1}) + \Delta t(\rho - \beta_2)\left\|v^{n+1}\right\|^2 + \Delta t\beta_1(u^{n+1}, v^{n+1}) \\
&\quad - \Delta t(k(c^n)v^{n+1}, v^{n+1}), \\
\left\|c^{n+1}\right\|^2 &= (c^n, c^{n+1}) - \Delta t\left\|\sqrt{D_c}\nabla c^{n+1}\right\|^2 \\
&\quad - \Delta t\left(\frac{k(c^{n+1})(u^{n+1} + v^{n+1})}{\alpha} - g(t_{n+1}), c^{n+1}\right) - \Delta tM\left\|c^{n+1}\right\|^2.
\end{aligned} \tag{41}$$

Using

$$(w, z) \le \frac{1}{2}(\|w\|^2 + \|z\|^2), \ w, z \in V_h \tag{42}$$

and (11), it holds for system (41) that

$$\begin{aligned}
(1 + \Delta t(2\beta_1 - \beta_2))\left\|u^{n+1}\right\|^2 &\le \|u^n\|^2 - 2\Delta t\,\delta\left\|\nabla u^{n+1}\right\|^2 + \Delta t\beta_2\left\|v^{n+1}\right\|^2 \\
&\quad - 2\Delta t(k(c^n)u^{n+1}, u^{n+1}) \\
&\quad + 2\Delta t^2\sum_{i=1}^{n+1}\ker(t_{n+1} - t_i)(D_v\nabla u^i, \nabla u^{n+1}), \\
(1 + \Delta t(2(\beta_2 - \rho) - \beta_1))\left\|v^{n+1}\right\|^2 &\le \|v^n\|^2 + \Delta t\beta_1\left\|u^{n+1}\right\|^2 \\
&\quad - 2\Delta t(k(c^n)v^{n+1}, v^{n+1}), \\
(1 + 2\Delta tM)\left\|c^{n+1}\right\|^2 &\le \|c^n\|^2 - 2\Delta t\,\delta\left\|\nabla c^{n+1}\right\|^2 \\
&\quad - 2\Delta t\left(\frac{k(c^{n+1})(u^{n+1} + v^{n+1})}{\alpha}, c^{n+1}\right) \\
&\quad - 2\Delta t(g(t_{n+1}), c^{n+1}).
\end{aligned} \tag{43}$$

The lower bound for k implies that

$$-(k(c^i)q, q) \le 0,$$

Proof of Theorem 4: Following the proof of Theorem 3, it can be established that

$$P_e(n) = P_t\rho n - \mu\sum_{j=0}^{n-1}\int_{jP_t}^{(j+1)P_t}\frac{c(s)}{k_d + c(s)}ds. \tag{37}$$

Using the ordinary differential equation satisfied by c,

$$c'(s) = -Mc(s) + g(s),\ s \in (0,T),$$

the integral in equation (37) can be calculated as

$$\begin{aligned}\int_{jP_t}^{(j+1)P_t}&\frac{c(s)}{k_d + c(s)}ds \\ &= \frac{1}{M}\left(\log\left(\frac{k_d + c((j+1)P_t)}{k_d + c(jP_t)}\right) - \sum_{i=0}^{m-1}\int_{jP_t+i}^{jP_t+i+\Delta t}\frac{d}{k_d + c(s)}ds\right).\end{aligned} \tag{38}$$

The summation of the first term in (38) can be directly computed as

$$\sum_{j=0}^{n-1}\log\left(\frac{k_d + c((j+1)P_t)}{k_d + c(jP_t)}\right) = \log\left(1 + \frac{c(nP_t)}{k_d}\right) = \log\left(1 + \frac{B(n)e^{-nP_tM}}{k_d}\right). \tag{39}$$

Regarding the second term in (38), using the upper bound

$$c(s) \le e^{-Ms}B(j+1),\ s \in [jP_t, (j+1)P_t],$$

it follows that

$$-\sum_{i=0}^{m-1}\int_{jP_t+i}^{jP_t+i+\Delta t}\frac{d}{k_d + c(s)}ds \le -\sum_{i=0}^{m-1}\int_{jP_t+i}^{jP_t+i+\Delta t}\frac{d}{k_d + e^{-Ms}B(j+1)}ds. \tag{40}$$

Calculating this last integral exactly, the upper bound for $P_e(n)$ follows. ∎

where E_0 represents the Young modulus of the Hookean spring and E_1, μ_1 represent, respectively, the Young modulus and the viscosity of the Kelvin body. Integrating (6) we obtain

$$\sigma(t) = e^{-\beta t}\sigma(0) + \int_0^t e^{-\beta(t-s)}\left(\alpha_1\varepsilon(s) + \alpha_2\frac{\partial\varepsilon}{\partial t}(s)\right)ds. \tag{7}$$

However, we note that a relation between the stress σ and the strain ε must reflect the fact that the two entities act in opposite directions, that is, that they have opposite signs. We now relate the strain ε with the density of cells of migratory phenotype u, by considering the *ansatz*

$$\varepsilon = \lambda u \tag{8}$$

where λ stands for a positive constant. Defining σ by the symmetric of the right hand side of (7) and replacing (4)-(8) in (3) we finally obtain

$$J_u(t) = -(\tilde{D} - \lambda E_0\tilde{D}_v)\nabla u(t) - \int_0^t \lambda\tilde{D}_v\frac{E_0^2}{\mu_1}e^{-\frac{E_0+E_1}{\mu_1}(t-s)}\nabla u(s)\,ds. \tag{9}$$

Let us represent in (9) the effective fickian diffusion by D, that is,

$$D = \tilde{D} - \lambda E_0\tilde{D}_v.$$

and let us denote by $D_v = -\lambda\tilde{D}_v\frac{E_0^2}{\mu_1}$, the nonfickian counterpart. We stress that since $\tilde{D}_v$ has negative diagonal entries, the contribution of the diffusion tensor D increases with increasing stiffness E_0.

From (1), (2) and (9), we have

$$\begin{cases}\dfrac{\partial u}{\partial t}(t) = \nabla\cdot\big(D\nabla u(t)\big) - \displaystyle\int_0^t \ker(t-s)\nabla\cdot\big(D_v\nabla u(s)\big)ds \\ \qquad\qquad - \beta_1 u(t) + \beta_2 v(t) - k(c(t))u(t), \\ \dfrac{\partial v}{\partial t}(t) = \rho v(t) + \beta_1 u(t) - \beta_2 v(t) - k(c(t))v(t), \\ \dfrac{\partial c}{\partial t}(t) = \nabla\cdot\big(D_c\nabla c(t)\big) - \dfrac{k(c(t))}{\alpha}(u(t) + v(t)) + g(t) - Mc(t),\end{cases} \tag{10}$$

in $\Omega\times(0,T]$, where $\ker(t) = e^{-\frac{t}{\tau}}$ and D, D_c, D_v are symmetric positive definite matrices, possibly space dependent.

We note that in [4] the authors, using a probabilistic approach with no relation with the mechanical point of view adopted in this work, established,

for the cells of migratory phenotype, an equation of the form

$$\frac{\partial u}{\partial t} = \frac{\sigma^2}{2}\int_0^t \ker(t-s)\Delta u(s)\,ds - \beta_1 u + \beta_2 v,$$

where $\ker(\cdot)$ represents a memory kernel defined in terms of a Laplace transform.

System (10) is closed with homogeneous Neumann boundary conditions

$$-\left(D\nabla u(t) - \int_0^t \ker(t-s)D_v\nabla u(s)ds\right)\cdot\eta = 0, \quad t>0$$

and

$$-D_c\nabla c(t)\cdot\eta = 0, \quad t>0,$$

where η represents the exterior unit normal, as well as suitable initial data.

We also assume that there exist $\delta,\lambda>0$ such that

$$\delta\left\|x\right\|_2^2 \leqslant (Dx,x) \leqslant \lambda\left\|x\right\|_2^2, \quad \forall x\in\mathbb{R}^d \tag{11}$$

and that D_v and D_c satisfy the same bounds.

We start by establishing an upper bound for the following energy functional

$$\begin{aligned}\mathbb{E}_{u,v,c}(t) &= \left\|u(t)\right\|^2 + \left\|v(t)\right\|^2 + \left\|c(t)\right\|^2 \\ &\quad + (2\delta-\epsilon^2\lambda)\int_0^t \left\|\nabla u(s)\right\|^2 ds + 2\delta\int_0^t \left\|\nabla c(s)\right\|^2 ds, \quad t\geq 0\end{aligned}$$

where $\epsilon\neq 0$, satisfying $2\delta-\epsilon^2\lambda>0$, is constructed in the proof of Theorem 1. Let $V_1 = L^2(0,T;H^1(\Omega))\cap H^1(0,T;L^2(\Omega))$, $Q = H^1(0,T;L^2(\Omega))$ and $V = V_1\times Q\times V_1$.

Theorem 1. *Let $(u,v,c)\in V$ be a solution of (10) and $k\in L^\infty(\mathbb{R}^+)$. Then there exists $\epsilon\neq 0$ such that $2\delta-\epsilon^2\lambda>0$ and*

$$\mathbb{E}_{u,v,c}(t) \leq e^{2Ct}\left(\left\|u_0\right\|^2 + \left\|v_0\right\|^2\right) + \int_0^t e^{-2C(s-t)}\left\|g(s)\right\|^2 ds$$

where

$$C = \max\left\{\frac{\beta_2-\beta_1}{2} + \frac{\left\|k\right\|_\infty^2}{\alpha^2}, \rho + \frac{\beta_1-\beta_2}{2} + \frac{\left\|k\right\|_\infty^2}{\alpha^2}, 1-M, \frac{\lambda\left\|\ker\right\|_{L^2(\mathbb{R}^+)}^2}{2\epsilon^2(2\delta-\epsilon^2\lambda)}\right\}.$$

A proof of Theorem 1 is presented in Appendix B.

Since system (10) is nonlinear, Theorem 1 does not imply the stability of its solution. The following result establishes this property.

It follows that

$$\begin{aligned}P_e(n) &= \rho n P_t - \frac{\mu}{c_0}\int_0^{nP_t}\int_0^s g(\tau)e^{M(\tau-s)}d\tau ds \\ &= \rho n P_t - \frac{\mu}{c_0}\sum_{j=0}^{n-1}\int_{jP_t}^{(j+1)P_t}\int_0^s g(\tau)e^{M(\tau-s)}d\tau ds.\end{aligned} \tag{32}$$

Using integration by parts, for each month j we have

$$\begin{aligned}&\int_{jP_t}^{(j+1)P_t}\int_0^s g(\tau)e^{M(\tau-s)}d\tau ds \\ =\ &\int_{jP_t}^{(j+1)P_t} e^{-Ms}\int_0^s g(\tau)e^{M\tau}d\tau ds \\ =\ &\frac{e^{-jP_tM}}{M}\Big(\int_0^{jP_t} g(\tau)e^{M\tau}d\tau - e^{-P_tM}\int_0^{(j+1)P_t} g(\tau)e^{M\tau}d\tau\Big) \\ &+\frac{1}{M}\int_{jP_t}^{(j+1)P_t} g(s)ds.\end{aligned} \tag{33}$$

For the first integral of (33), doing the summation for the geometric progressions, we have

$$\int_0^{jP_t} g(\tau)e^{M\tau}d\tau \ = \ \frac{d(e^{\Delta tM}-1)}{M}\frac{1-e^{jP_tM}}{1-e^{P_tM}}\frac{1-e^{mM}}{1-e^{M}} = B(j). \tag{34}$$

For the third integral of (33), we have

$$\int_{jP_t}^{(j+1)P_t} g(s)ds = dm\Delta t = d_{total}. \tag{35}$$

Using (34) and (35) on (33), we get

$$\begin{aligned}&\int_{jP_t}^{(j+1)P_t}\int_0^s g(\tau)e^{M(\tau-s)}d\tau ds \\ =\ &\frac{d}{M^2}\frac{1-e^{mM}}{1-e^{M}}\frac{1}{1-e^{P_tM}}\big(e^{\Delta tM}-1\big)e^{-jP_tM}\big(1-e^{-P_tM}\big) + \frac{d_{total}}{M}\end{aligned} \tag{36}$$

and so, from (32) and doing the summation for the geometric progression, we finally get (19).

■

and

$$-\left(k(\tilde{c}(t))\tilde{v}(t)-k(c(t))v(t),\overline{v}(t)\right)$$
$$\leq\left(\|k\|_{\infty}+\frac{\|k'\|_{\infty}\|v(t)\|_{\infty}^{2}}{2}\right)\|\overline{v}(t)\|^{2}+\frac{\|k'\|_{\infty}\|v(t)\|_{\infty}^{2}}{2}\|\overline{c}(t)\|^{2}$$

and also

$$-\left(k(\tilde{c}(t))(\tilde{u}(t)+\tilde{v}(t))-k(c(t))(u(t)+v(t)),\overline{c}(t)\right)$$
$$\leq\frac{\|k\|_{\infty}}{2}\left(\|\overline{u}(t)\|^{2}+\|\overline{v}(t)\|^{2}\right)+\left(\|k\|_{\infty}+\|k'\|_{\infty}\|u(t)+v(t)\|_{\infty}\right)\|\overline{c}(t)\|^{2}.$$

Let

$$C_1(u)=\frac{C_e^2}{2}\|k'\|_{\infty}\|u\|^2_{L^{\infty}(0,T,L^{\infty}(\Omega))},\qquad C_2(u)=\|k\|_{\infty}+C_1(u),$$

for $u\in V_1\cap L^{\infty}(0,T,L^{\infty}(\Omega))$. Using these notations, the previous inequalities can be bounded by constants that do not depend on t:

$$-\left(k(\tilde{c}(t))\tilde{u}(t)-k(c(t))u(t),\overline{u}(t)\right)\leq C_1(u)\|\overline{c}(t)\|^2+C_2(u)\|\overline{u}(t)\|^2$$

and

$$-\left(k(\tilde{c}(t))\tilde{v}(t)-k(c(t))v(t),\overline{v}(t)\right)\leq C_1(v)\|\overline{c}(t)\|^2+c(v)\|\overline{v}(t)\|^2,$$

and also

$$-\left(k(\tilde{c}(t))(\tilde{u}(t)+\tilde{v}(t))-k(c(t))(u(t)+v(t)),\overline{c}(t)\right)$$
$$\leq\frac{\|k\|_{\infty}}{2}\left(\|\overline{u}(t)\|^{2}+\|\overline{v}(t)\|^{2}\right)+2c(u+v)\|\overline{c}(t)\|^{2}.$$

The proof follows now the same guidelines as the one for Theorem 1, with

$$C=\max\left\{\beta_2-\beta_1+2C_2(u)+\frac{2}{\alpha}\|k\|_{\infty},2\rho+\beta_1-\beta_2+2c(v)+\frac{2}{\alpha}\|k\|_{\infty},\right.$$
$$\left.2\left(C_1(u)+C_1(v)+M\right)+\frac{4}{\alpha}C_2(u+v),\frac{\lambda\|\ker\|^2_{L^2(\mathbb{R}^+)}}{2\epsilon^2(2\delta-\epsilon^2\lambda)}\right\}.$$

■

Proof of Theorem 3: Combining the definition of P_e and (17) we obtain

$$P_e(n)=\int_0^{nP_t}\left(\rho-\frac{\mu}{c_0}\int_0^s g(\tau)e^{M(\tau-s)}d\tau\right)ds.$$

Theorem 2. *Let $(u,v,c)\in V\cap[L^{\infty}(0,T,L^{\infty}(\Omega))]^3$ denote a solution of system (10) and $(\tilde{u},\tilde{v},\tilde{c})\in V$ a perturbation with different initial data. If $k\in W^{1,\infty}(\mathbb{R}^+)$ then there exists $C>0$ such that*

$$\mathcal{M}(t)\leq C\mathcal{M}(0),\ t\in[0,T] \tag{12}$$

where

$$\mathcal{M}(t)=\|\tilde{u}(t)-u(t)\|^2+\|\tilde{v}(t)-v(t)\|^2+\|\tilde{c}(t)-c(t)\|^2,\ t\in[0,T].$$

A proof of Theorem 2 is presented in Appendix B.

3. Treatment protocols for chemotherapy

The estimates established in the previous section are not useful to define treatment protocols, i.e., to calculate the dosage and frequency of treatment that lead to control the tumour mass. However, this task can be accomplished by simplifying system (10) and determining convenient upper bounds for the mass of tumour cells.

The approach that we follow in this section analyses a more general case than the one presented in [2]. Following a similar approach, we assume

(1) u, v and c are nonnegative,
(2) drug dynamics is dominated by delivery, ie, $D_c=0$ and
(3) $\frac{k}{\alpha}\approx 0$ (simplification based on real data).

Let

$$\mathbb{M}(t)=\int_{\Omega}\big(u(t)+v(t)\big)d\Omega, \tag{13}$$

define the total mass of tumour cells at time $t\geq 0$.

Combining the equations of (10) and the homogeneous boundary conditions we get

$$\mathbb{M}'(t)=\rho\int_{\Omega}vd\Omega-\int_{\Omega}k(c)(u+v)d\Omega, \tag{14}$$

which leads to

$$\mathbb{M}(t)\leq\mathbb{M}(0)e^{\int_0^t(\rho-k(c(s)))ds}. \tag{15}$$

When chemotherapy is applied, condition (15) can be used to determine an effective dosage such that the total amount of tumour cells do not increase. In fact, if

$$\int_0^t\left(\rho-k\left(c(s)\right)\right)ds\leq 0, \tag{16}$$

then we can conclude that $\mathbb{M}(t)\leq\mathbb{M}(0)$, at any time t.

From hypothesis 2 and 3, the drug concentration equation has a solution given by

$$c(t) = \int_0^t e^{-M(t-s)} g(s) ds + e^{-Mt} c(0). \tag{17}$$

A typical protocol in chemotherapy treatment follows the bang-bang approach, which alternates maximum doses of chemotherapy with rest periods when no drug is administered. In this treatment, function g, that represents the concentration of release drug per unit of time, is defined by

$$g(t) = \begin{cases} d, \text{ when chemotherapy is being administered} \\ 0, \text{ otherwise} \end{cases} \tag{18}$$

for $t \geqslant 0$.

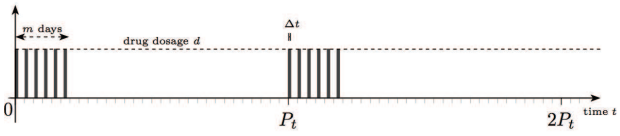

FIGURE 2. Chemotherapy protocol.

In the definition of the treatment protocol, we consider the following variables and assumptions:

- each treatment cycle (chemotherapy sessions and rest period) has P_t days;
- the patient is submitted to m chemotherapy sessions during each treatment cycle, on the first $m(\leq P_t)$ consecutive days of the latter;
- each chemotherapy session has a time duration $\Delta t(\leq 24h)$;
- in each chemotherapy session the patient receives a drug dose $d \cdot \Delta t = \frac{d_{total}}{m}$, where d_{total} represents the total dosage of drug to be administered in one month;
- the chemotherapy protocol will be repeated for n months.

In Figure 2 we present an example of a protocol with $m = 6$ chemotherapy sessions each month.

For $t = nP_t$, let us represent the first member of (16) by $P_e(n)$. In the following we establish upper bounds for $P_e(n)$ considering two different expressions for the function k:

$$k(c) = \frac{\mu}{c_0} c \quad \text{(linear model)}$$

and consequently

$$\frac{\mathrm{d}\mathbb{E}_{u,v,c}}{\mathrm{d}t}(t) \leq 2C\mathbb{E}_{u,v,c}(t) + \|g(t)\|^2, \tag{31}$$

which concludes the proof. ∎

Proof of Theorem 2: Let $\overline{u}(t) = \tilde{u}(t) - u(t)$, $\overline{v}(t) = \tilde{v}(t) - v(t)$, $\overline{c}(t) = \tilde{c}(t) - c(t)$, for $t \in \mathbb{R}_0^+$. Since (u, v, c) and $(\tilde{u}, \tilde{v}, \tilde{c})$ satisfy (10) and using (28) it follows that there exists $\epsilon \neq 0$ such that

$$\begin{aligned} &\frac{1}{2}\frac{\mathrm{d}}{\mathrm{d}t}\|\overline{u}(t)\|^2 + \left(\delta - \frac{\epsilon^2\lambda}{2}\right)\|\nabla\overline{u}(t)\|^2 \\ &\qquad \leq -\beta_1\|\overline{u}(t)\|^2 + \frac{\lambda\|\ker\|^2_{L^2(\mathbb{R}^+)}}{2\epsilon^2}\int_0^t \|\nabla\overline{u}(s)\|^2 ds \\ &\qquad\qquad + \beta_2(\overline{v}(t), \overline{u}(t)) - (k(\tilde{c}(t))\tilde{u}(t) - k(c(t))u(t), \overline{u}(t)) \end{aligned}$$

and

$$\frac{1}{2}\frac{\mathrm{d}}{\mathrm{d}t}\|\overline{v}(t)\|^2 = (\rho - \beta_2)\|\overline{v}(t)\|^2 + \beta_1(\overline{u}(t), \overline{v}(t)) - (k(\tilde{c}(t))\tilde{u}(t) - k(c(t))u(t), \overline{u}(t))$$

and also

$$\begin{aligned} &\frac{1}{2}\frac{\mathrm{d}}{\mathrm{d}t}\|\overline{c}(t)\|^2 + \delta\|\nabla\overline{c}(t)\|^2 \\ &\qquad \leq M\|\overline{c}(t)\|^2 - \frac{1}{\alpha}(k(\tilde{c}(t))(\tilde{u}(t) + \tilde{v}(t)) - k(c(t))(u(t) + v(t)), \overline{c}(t)). \end{aligned}$$

The treatment of the linear terms of the equations that arise uses the same technique used in Theorem 1. To establish the desired inequality, it remains to bound the nonlinear terms.

A quick calculation shows that

$$\begin{aligned} &-(k(\tilde{c}(t))\tilde{u}(t) - k(c(t))u(t), \overline{u}(t)) \\ &\qquad \leq \|k\|_\infty\|\overline{u}(t)\|^2 + \|k'\|_\infty\|u(t)\|^2_\infty\|\overline{c}(t)\|\,\|\overline{u}(t)\| \\ &\qquad \leq \left(\|k\|_\infty + \frac{\|k'\|_\infty\|u(t)\|^2_\infty}{2}\right)\|\overline{u}(t)\|^2 + \frac{\|k'\|_\infty\|u(t)\|^2_\infty}{2}\|\overline{c}(t)\|^2 \end{aligned}$$

Combining (24), (25) and (26) and using bounds (11) we get

$$\begin{aligned}
&\frac{1}{2}\frac{\mathrm{d}}{\mathrm{d}t}\left(\|u(t)\|^2+\|v(t)\|^2+\|c(t)\|^2+2\delta\int_0^t\|\nabla u(s)\|^2\,ds+2\delta\int_0^t\|\nabla c(s)\|^2\,ds\right)\\
&\leq-\beta_1\|u(t)\|^2+(\beta_2+\beta_1)(v(t),u(t))+(\rho-\beta_2)\|v(t)\|^2-(k(c(t))u(t),u(t))\\
&-(k(c(t))v(t),v(t))-\left(\frac{k(c(t))}{\alpha}(u(t)+v(t)),c(t)\right)+(g(t),c(t))-M\|c(t)\|^2\\
&\qquad+\int_0^t\ker(t-s)(D_v\nabla u(s)ds,\nabla u(t))ds. \quad (27)
\end{aligned}$$

For the last integral in (27), there exists $\epsilon\neq 0$ such that

$$\begin{aligned}
&\int_0^t\ker(t-s)(D_v\nabla u(s)ds,\nabla u(t))ds\\
&\qquad\leq\frac{\epsilon^2\lambda}{2}\|\nabla u(t)\|^2+\frac{\lambda\|\ker\|^2_{L^2(\mathbb{R}^+)}}{2\epsilon^2}\int_0^t\|\nabla u(s)\|^2\,ds. \quad (28)
\end{aligned}$$

Chosing ϵ such that $2\delta-\epsilon^2\lambda>0$, (27) becomes

$$\begin{aligned}
\frac{1}{2}\frac{\mathrm{d}\mathbb{E}_{u,v,c}}{\mathrm{d}t}(t)&\leq-\beta_1\|u(t)\|^2+(\beta_2+\beta_1)(v(t),u(t))+(\rho-\beta_2)\|v(t)\|^2\\
&-(k(c(t))u(t),u(t))-(k(c(t))v(t),v(t))\\
&-\left(\frac{k(c(t))}{\alpha}(u(t)+v(t)),c(t)\right)\\
&+(g(t),c(t))-M\|c(t)\|^2+\frac{\lambda\|\ker\|^2_{L^2(\mathbb{R}^+)}}{2\epsilon^2}\int_0^t\|\nabla u(s)\|^2\,ds. \quad (29)
\end{aligned}$$

Applying Cauchy-Schwartz and Young's inequalities to the inner products in (29), it follows that

$$\begin{aligned}
\frac{1}{2}\frac{\mathrm{d}\mathbb{E}_{u,v,c}}{\mathrm{d}t}(t)&\leq\left(\frac{\beta_2-\beta_1}{2}+\frac{\|k\|^2_\infty}{\alpha^2}\right)\|u(t)\|^2+\left(\rho+\frac{\beta_1-\beta_2}{2}+\frac{\|k\|^2_\infty}{\alpha^2}\right)\|v(t)\|^2\\
&+(1-M)\|c(t)\|^2+\frac{1}{2}\|g(t)\|^2+\frac{\lambda\|\ker\|^2_{L^2(\mathbb{R}^+)}}{2\epsilon^2}\int_0^t\|\nabla u(s)\|^2\,ds \quad (30)
\end{aligned}$$

and

$$k(c)=\mu\frac{c}{k_d+c}\quad\text{(Michaelis-Menten model)},$$

for $c\in\mathbb{R}_0^+$, where μ is a measure of the effectiveness of the drug, c_0 is the maximum external drug concentration and k_d is a critical drug concentration. We remark that the choice for k depends on the type of drug-cell kinetics, as experimental evidence suggests [17]. In Figure 3 we plot the qualitative behaviour of k for both cases.

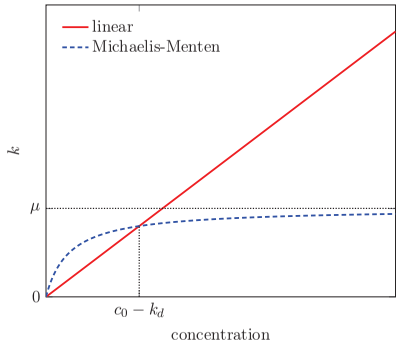

FIGURE 3. Plot of the linear and Michaelis-Menten representations of k.

From a mathematical point of view, it is clear that both expressions induce different behaviours in the drug-cell kinetics. On one hand, for large values of the concentration, while the nonlinear (Michaelis-Menten model) remains bounded by μ, the linear one is not. On the other hand, the Michaelis-Menten model describes a higher rate of killed cells for low values of the concentration.

Theorem 3. *If k is a linear function of c, i.e., if $k(c)=\frac{\mu}{c_0}c$, for $\mu,c_0>0$, then*

$$P_e(n)=P_t\rho\,n-\mu\frac{d_{total}\,n}{Mc_0}+\mu\frac{B(n)e^{-nP_tM}}{Mc_0} \quad (19)$$

where

$$B(j)=\frac{d_{total}}{m\Delta t}\frac{e^{\Delta tM}-1}{M}\frac{1-e^{jMP_t}}{1-e^{P_tM}}\frac{1-e^{mM}}{1-e^{M}},\quad j=0,1,\ldots,n. \quad (20)$$

A proof of Theorem 3 is presented in Appendix B.

If the expression of k is nonlinear in c, the previous technique for calculating $P_e(n)$ cannot be used. In the following result we establish an upper bound for $P_e(n)$ when the Michaelis-Menten model is considered.

Theorem 4. *Let $\mu, k_d > 0$. If $k(c) = \mu \frac{c}{k_d + c}$ then*

$$P_e(n) \leq P_t \rho\, n - \frac{\mu}{k_d} \frac{d_{total}}{m \Delta t\, M^2} \sum_{j=0}^{n-1} \sum_{i=0}^{m-1} \log\left(\frac{k_d e^{M\Delta t} + B(j+1) e^{-M(jP_t+i)}}{k_d + B(j+1) e^{-M(jP_t+i)}} \right) + \frac{\mu}{M} \log\left(1 + \frac{B(n) e^{-MnP_t}}{k_d} \right) \tag{21}$$

where $B(j)$ is defined as (20).

A proof of Theorem 4 is presented in Appendix B.

To guarantee that $P_e(n) \leq 0$, depending on the function k being considered, we can use (19) or (21) to determine an effective dosage d_{total} and the frequency of treatments that allows to control the total tumour mass. Obviously the value of d_{total} depends on the chemotherapy protocol chosen.

4. Numerical method

We now present a numerical scheme to approximate the solution of the proposed problem. Let N denote a positive integer. We define $\Delta t = \frac{T}{N}$ and introduce the uniform partition in $[0, T]$, $t_i = i\Delta t, i = 0, \ldots, N$. Let $h > 0$ denote a fixed parameter and $\mathcal{T}_h$ an admissible triangulation of the domain Ω where

$$h = \max_{K \in \mathcal{T}_h} \operatorname{diam}(K)$$

and $\operatorname{diam}(K)$ denotes the diameter of triangle K.

Let V_h denote the space of piecewise linear functions built upon $\mathcal{T}_h$, that is,

$$V_h = \{ v \in C^0(\overline{\Omega}) : v_{|K} \in \mathbb{P}_1(K), K \in \mathcal{T}_h \},$$

where $\mathbb{P}_1(K)$ denotes the space of polynomials of degree at most one, defined in K.

Discretizing system (10) with an implicit-explicit strategy in time and the finite element method in space, we establish the following variational

Relaxation parameter	β^{-1}	$0.00348\, day$	[1, 7]
Nonfickian diffusion coefficient	D_v	$0.001\, cm^2/day^2$	[1, 7]
Diffusion coefficient (drug)	D_c	$0.432\, cm^2/day$	[10]
Total drug concentration	d_{total}	$0.12\, g/cm^2$	-
Critical drug concentration	k_d	$2 \cdot 10^{-6}\, g/cm^2$	[10]
Metabolic removal rate	M	$9.242\, /day$	-

Appendix B. Proof of theoretical results

Proof of Theorem 1: From the first equation, we have

$$\begin{aligned} \frac{1}{2}\frac{\mathrm{d}}{\mathrm{d}t}\left(\|u(t)\|^2 + 2\int_0^t \left\| \sqrt{D}\nabla u(s) \right\|^2 ds \right) &= -\beta_1 \|u(t)\|^2 + \beta_2 (v(t), u(t)) - (k(c(t))u(t), u(t)) \\ &\quad + \int_0^t \ker(t-s)(D_v \nabla u(s) ds, \nabla u(t)) ds. \end{aligned} \tag{24}$$

From the second equation, it follows

$$\frac{1}{2}\frac{\mathrm{d}}{\mathrm{d}t} \|v(t)\|^2 \leq (\rho - \beta_2) \|v(t)\|^2 + \beta_1 (u(t), v(t)) - (k(c(t))v(t), v(t)). \tag{25}$$

From the third equation, we have

$$\begin{aligned} \frac{1}{2}\frac{\mathrm{d}}{\mathrm{d}t} \|c(t)\|^2 = -\left\| \sqrt{D_c}\nabla c(t) \right\|^2 - \left(\frac{k(c)}{\alpha}(u(t) + v(t)), c(t) \right) \\ + (g(t), c(t)) - M \|c(t)\|^2. \end{aligned} \tag{26}$$

regularity assumptions. A numerical method based on finite differences and finite elements is proposed and its stability properties are analysed.

In order to study the total mass of tumour cells in the system, suitable indicators for the chemotherapy protocol's efficiency are established. Under sufficient conditions on the (controllable) parameters of the system, the controlled growth of tumour mass is achieved. Using these indicators, three different chemotherapy protocol scenarios are proposed and analysed, considering a linear and nonlinear (Michaelis-Menten model) representation for the function governing the drug-cell kill interaction. Depending on the dynamics of this interaction, our numerical simulations show different behaviours: for the linear model, more treatment sessions do not have an impact on the growth control; in the Michaelis-Menten model, more frequent chemotherapy sessions with less aggressive dosages might be preferable. These last results are in agreement with new medical research in metronomics chemotherapy, based on more frequent treatments with low doses administration.

Appendix

Appendix A. Simulation parameters

Parameter	Symbol	Value	Ref.
Growth rate	ρ	$0.012\,/day$	[12]
Switching parameters	β_1	$10^{-6}\,/day$	[12]
	β_2	$0.036\,/day$	[12]
Fickian diffusion coefficient (gray matter)	D_g	$0.0013\,cm^2/day$	[12, 14]
Fickian diffusion coefficient (white matter)	D_w	$5 \cdot D_g\,cm^2/day$	[12, 14]
Measure of the rate of cell kill relative to the rate of drug degradation	α	$24 \times 10^{10}\,ml/(g\,cm^2)$	[10]
Maximum external drug concentration	c_0	$10^{-5}\,g/cm^2$	[10]

formulation for the discrete problem: find $u^{n+1}, v^{n+1}, c^{n+1} \in V_h$ such that

$$\begin{aligned}
\left(\frac{u^{n+1}-u^n}{\Delta t}, w\right) &= -(D\nabla u^{n+1}, \nabla w) + (-\beta_1 u^{n+1} + \beta_2 v^{n+1} - k(c^n)u^{n+1}, w) \\
&\quad + \Delta t \sum_{i=1}^{n+1} \ker(t_{n+1}-t_i)(D_v \nabla u^i, \nabla w), \\
\left(\frac{v^{n+1}-v^n}{\Delta t}, z\right) &= (\rho v^{n+1} + \beta_1 u^{n+1} - \beta_2 v^{n+1} - k(c^n)v^{n+1}, z), \\
\left(\frac{c^{n+1}-c^n}{\Delta t}, q\right) &= -(D_c \nabla c^{n+1}, \nabla q) \\
&\quad + \left(g(t_{n+1}) - \frac{k(c^{n+1})(u^{n+1}+v^{n+1})}{\alpha} - M c^{n+1}, q\right)
\end{aligned} \tag{22}$$

for all $w, z, q \in V_h$.

We remark that the solution of system (22) can be obtained by a decoupling strategy: first we solve for the first two equations (simultaneously) and then we calculate the approximate concentration.

The numerical scheme can also be studied from a stability point of view, as it was the case of the continuous model. We start by establishing an upper bound for an energy of the solution of scheme (22).

Theorem 5. *Let*

$$C_1 = \min\left\{\beta_1 - \beta_2 - \frac{\|k\|_\infty}{\alpha}, \beta_2 - \beta_1 - 2\rho - \frac{\|k\|_\infty}{\alpha}, 2M - \|k\|_\infty\left(\frac{2}{\alpha}+1\right)\right\}.$$

If $k \in L^\infty(\mathbb{R}^+)$, $g \in C^0([0,T])$, Δt *is such that* $1 + \Delta t C_1$ *and*

$$C = 2\,\delta - 2\lambda\left(\Delta t + \frac{\|\ker\|^2_{L^2(\mathbb{R}^+)}}{2}\right)$$

are positive then, for

$$C_2 = \frac{\lambda(\Delta t + \|\ker\|^2_{L^2(\mathbb{R}^+)})}{C}$$

method (22) *verifies the following bound*

$$\mathbb{E}_n \leq e^{n\frac{C_2 - C_1\Delta t}{1+\Delta t C_1}}\,\mathbb{E}_0 + \Delta t(\mathrm{meas}(\Omega))^2 \sum_{i=0}^{n-1} \frac{1}{(1+\Delta t C_1)^{n-i}}\,(g(t_{i+1}))^2\,, \tag{23}$$

where

$$\mathbb{E}_n = \|u^n\|^2 + \Delta t\, C \sum_{i=1}^{n} \left\|\nabla u^i\right\|^2 + \|v^n\|^2 + \|c^n\|^2 + 2\Delta t\, \delta\, \|\nabla c^n\|^2$$

is a discrete version of $\mathbb{E}_{u,v,c}(t_n)$.

A proof of Theorem 5 is presented in Appendix B.

We remark that combining the treatment of the nonlinear terms presented in the proof of Theorem 2 with the technique followed in the proof of Theorem 5, we can establish the stability of the numerical solution, under a suitable condition on the parameters of the problem.

5. Numerical results and discussion

We now illustrate the behaviour of the solution of system (10) with the help of the numerical scheme (22). To this end, we have considered the computational domain, Ω, depicted in Figure 4b (approximately $14.4cm \times 9.2cm$). The coordinate system has its origin at the lower left corner of the image. The domain was discretized with a triangular mesh, see Figure 4a.

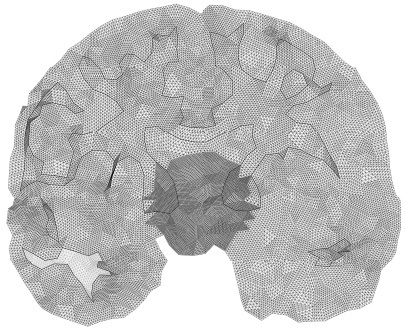

(A) Triangular mesh on the brain slice.

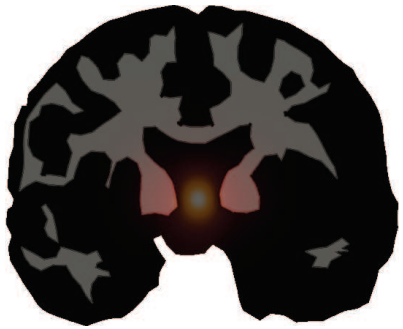

(B) White matter (dark grey) and grey matter (black) and initial gaussian profile for tumour cells.

FIGURE 4. Computational representation of the brain.

The initial condition was taken as

$$v_0(x,y) = 10^3 e^{-50((x-7.2)^4+(y-4.6)^4)}, \quad (x,y) \in \Omega,$$

reduction of tumour cells. In fact, even if a small amount of drug is present, the drug still maintains good effectiveness properties, in agreement with Figure 3.

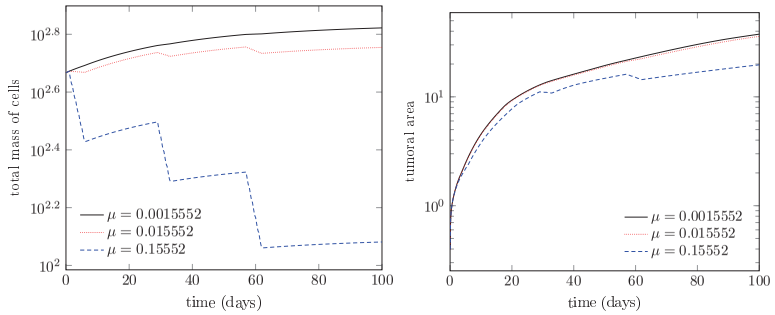

(A) Protocol II.

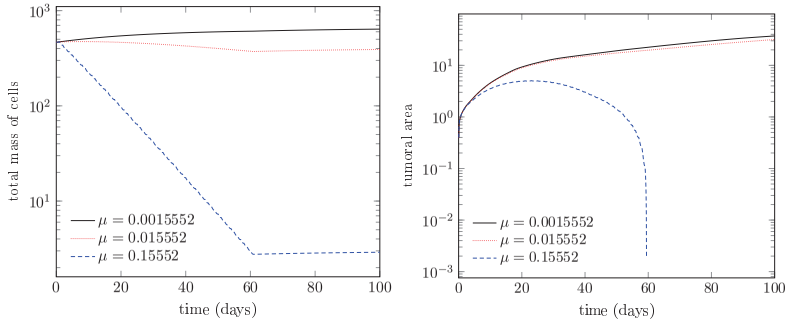

(B) Protocol III.

FIGURE 10. Plot of tumour mass and area for the nonlinear representation.

6. Conclusions

In this paper we propose a nonlinear mathematical model to describe the evolution of brain tumour cells with and without the effect of a chemotherapy drug. The stability of the solution of the model is established under convenient

The results in Figure 8 are in agreement with the data in Figure 6: the area of the tumour is higher for $\mu = 0.0015552$ and so is the cell density.

Comparing different protocols for the same drug effectiveness parameters, Figure 9 suggests that there is no direct relation between the number of sessions of chemotherapy and the protocol efficiency. Indeed, when we go from 5 sessions to 28 sessions, see Figure 9a, a more efficient control of the tumour mass does not emerge. Control is nonetheless present but the chemotherapy protocol does not reduce more the density of cells. Another interesting observation from Figure 9 is the change of growth rate of the diffusive tumour cells after each treatment cycle. In both drug effectiveness parameters, after each cycle, the rate decreases and this is due to the spatial distribution of the tumor.

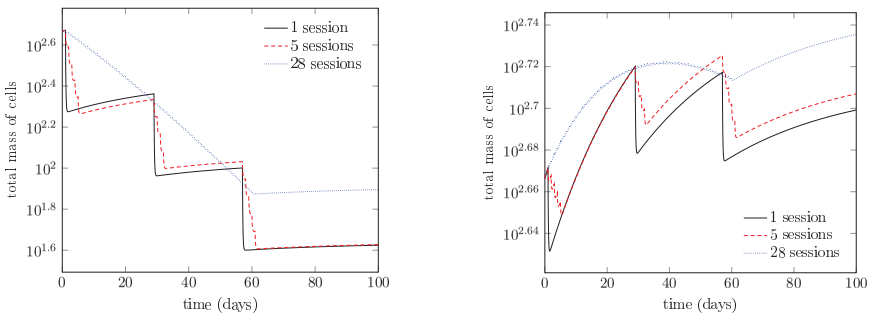

(A) $\mu = 0.015552$. (B) $\mu = 0.0015552$.

FIGURE 9. Plot of tumour mass and area for different drug effectiveness parameters for the linear representation.

The nonlinear representation of function k (Michaelis-Menten model) induces a different behaviour in the overall results. A first comment addresses the sharpness of the upper bound (21). From Figure 10 (left column), the decrease in the overall diffusive cells' density is present even if it was not guaranteed as such from Figure 5. This implies that the region in Figure 5 for which controlled tumour growth is larger than our estimate shows.

An interesting difference with respect to the linear case is the fact that in this scenario, the increased number of sessions leads to a better control (reduction) of the tumour density, even if this was not clear in the inequallity (21), see Figure 10a and 10b. This behaviour is explained by the way k acts on the

to emulate a tumoral mass centered in the geometry, as represented in Figure 4b. The mesh was refined near the peak of the gaussian profile in order to better capture the steep gradients. The complete list of all the parameters used in the simulation is found in Appendix A.

Remark 1. *The diffusion tensor is chosen to be diagonal where its nonzero entries are equal to D_g in the gray matter and D_w in the white matter.*

Remark 2. *The metabolic removal rate was calculated based on the biological half life of Temozolomide. The total amount of drug was fixed to illustrate the different behaviour of the solution, varying the efficacy of the drug.*

In what follows we analyse three different treatment protocols, for treatment cycles of length $P_t = 28$ days, considering $m = 1, 5, 28$ and the corresponding drug dosage (per unit of time), as detailed in Table 1.

	m	d
protocol I	1	0.12
protocol II	5	0.024
protocol III	28	0.0043

TABLE 1. Treatment protocol's definition.

From (19) and the upper bound (21), we plot in Figure 5 the dependency of these expressions with respect to to the number of monthly sessions of chemotherapy and the drug effectiveness parameter.

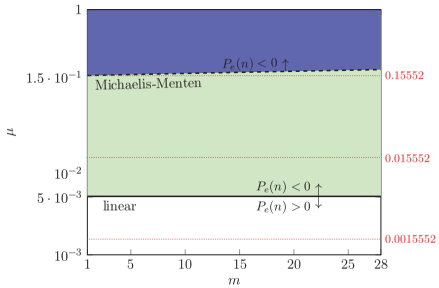

FIGURE 5. Admissible regions of controlled tumour growth.

The solid line corresponds to the protocol efficiency of the linear model while the dashed line corresponds to the upper bound for the Michaelis-Menten

model and is therefore only a sufficient condition to guarantee controlled tumour growth. Any choice of parameters μ and m that lies above the solid line (for the linear model) or dashed line (for the Michaelis-Menten model) leads to controlled growth for the respective representation. Also, from the plot, we can see that for the linear case, the protocol efficiency does not depend on the number of chemotherapy sessions. However, for the Michaelis-Menten model, the upper bound shows a slight dependency on m. In both cases, the protocol efficiency depends, as expected, on the drug effectiveness parameter. The results also suggest that, although the dashed line corresponds to an upper bound, the Michaelis-Menten model induces more restrictive choices for the drug in order to guarantee controlled growth.

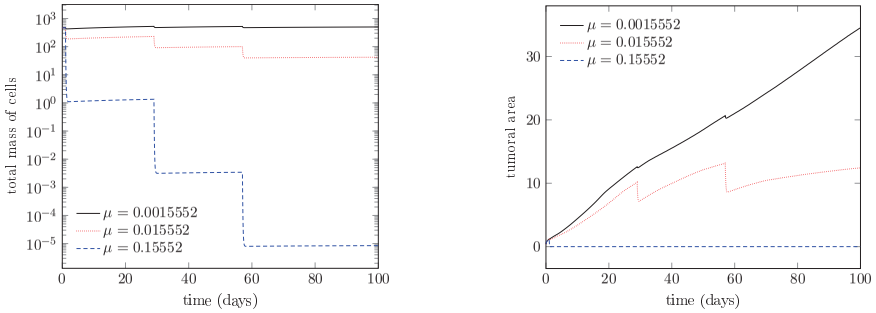

FIGURE 6. Plot of tumour mass and area for the linear representation for Protocol I.

Figure 5 also shows three dotted lines, that correspond to specific choices of the parameter μ. This choice was made in order to analyse the behaviour of the solutions under these different scenarios. While for $\mu = 0.0015552$, controlled growth is not guaranteed for both representations, for $\mu = 0.015552$ we can only assure control for the linear case. The other choice of the drug effectiveness parameter $\mu = 0.15552$ is such that control is established again for the linear model and also for protocol I with the Michaelis-Menten model. We stress that since we work with an upper bound for the Michaelis-Menten model, we cannot establish growth control for protocols II ($m = 5$) and III ($m = 28$). In order to clarify further this question, we conducted a series of numerical experiments that shall be detailed next.

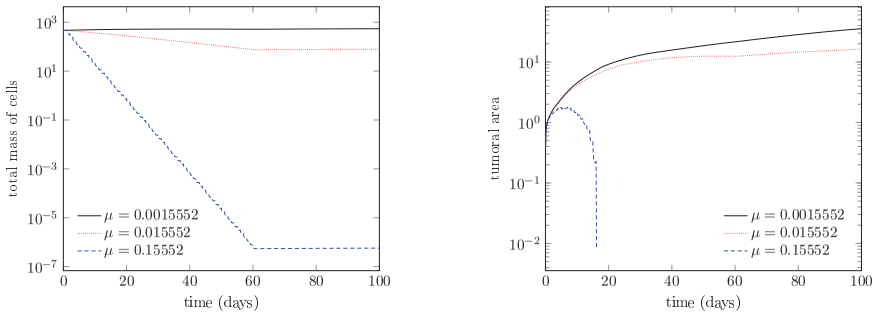

FIGURE 7. Plot of tumour mass and area for the linear representation for Protocol III.

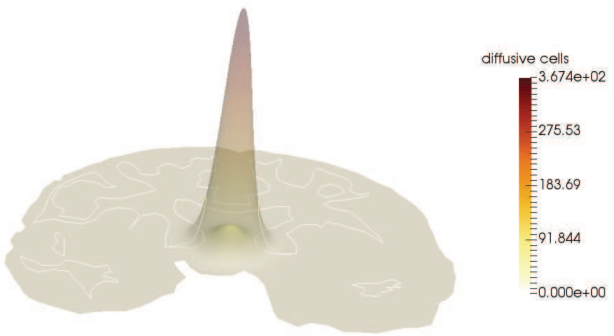

FIGURE 8. Plot of diffusive cells density for protocol I and drug effectiveness parameters $\mu = 0.015552$ and $\mu = 0.0015552$ ($t = 100\,days$).

The guarantee of growth control for the linear model for $\mu = 0.15552$ and $\mu = 0.015552$ is illustrated in Figures 6 and 7 (left column) for protocols I and III, respectively (the results for protocol II are similar to protocol I). We highlight that this bound does not amount to controlling the tumoral area, as seen on the right column of the same figure.

In Figure 8 we also show a plot with the diffusive cells distribution for protocol I and two different drug effectiveness parameters, $\mu = 0.015552$ and $\mu = 0.0015552$. The highest peak corresponds to the drug with the lowest drug effectiveness parameter (and for which growth control is not guaranteed).